Compound prism design principles, III: linear-in-wavenumber and optical coherence tomography prisms

Nathan Hagen[1,2] and Tomasz S. Tkaczyk[1,*]

[1]Department of Bioengineering, Rice University, Houston Texas 77005, USA

[2]e-mail:nhagen@optics.arizona.edu

*Corresponding author: ttkaczyk@rice.edu

Received 26 May 2011; accepted 5 July 2011;
posted 12 July 2011 (Doc. ID 148165); published 30 August 2011

We extend the work of the first two papers in this series [Appl. Opt. **50**, 4998–5011 (2011), Appl. Opt. **50**, 5012–5022 (2011)] to design compound prisms for linear-in-wavenumber dispersion, especially for application in spectral domain optical coherence tomography (OCT). These dispersive prism designs are believed to be the first to meet the requirements of high resolution OCT systems in direct-view geometry, where they can be used to shrink system size, to improve light throughput, to reduce stray light, and to reduce errors resulting from interpolating between wavelength- and wavenumber-sampled domains. We show prism designs that can be used for thermal sources or for wideband superluminescent diodes centered around wavelengths 850, 900, 1300, and 1375 nm.

OCIS codes: 230.5480, 080.2740, 260.2030, 300.6190, 110.4500.

1. Introduction

The first two papers of this series [1,2] (called Paper I and Paper II below) introduced basic design principles for compound prisms, concentrating on compact and linear-in-wavelength dispersive prisms. We showed that it is possible to achieve a degree of dispersion previously only thought possible with gratings, while maintaining direct-vision geometry. This characteristic is made possible by the underappreciated advantage that prisms have in design flexibility: with multiple surfaces and multiple glass choices available, an optical designer has multiple parameters to adjust for optimizing prism performance. Here we extend our design method to include prisms whose dispersion is linear in the wavenumber domain, and apply this method to the spectral ranges and high dispersion required by spectral domain optical coherence tomography (OCT) systems, an application that has previously been considered as too demanding for using prisms as dispersive elements. We show that not only can prisms replace gratings in this application, but that they can be used in direct-view geometry and provide better dispersion linearity in the wavenumber domain than gratings can.

2. Linear-in-Wavenumber Dispersion

Spectral interferometric applications typically find it desirable to have a spectrum which is sampled uniformly in the wavenumber rather than the uniformity in wavelength common to grating-based dispersive spectrometers, as this allows direct application of Fourier transform algorithms on the measured spectrum [3–5]. A spectrometer that samples the spectrum uniformly in the wavenumber domain requires a disperser whose ray deviation angle δ varies linearly with wavenumber σ, i.e., $\delta(\sigma) \propto \sigma$ for $\sigma = 1/\lambda$. The refractive index of typical glass has a nearly linear relationship with wavenumber, a characteristic where prisms have an advantage over gratings. Figure 1 shows the dispersion curve for SF66 glass and compares its linearity in both the wavelength and wavenumber domains with that of

0003-6935/11/255023-08$15.00/0

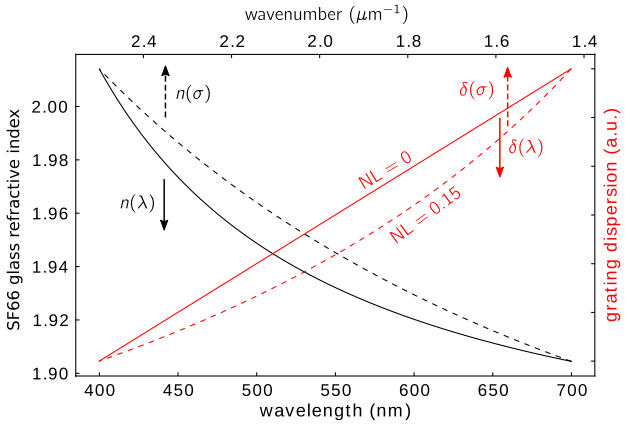

Fig. 1. (Color online) Dispersion of SF66 glass is substantially nonlinear when plotted against the wavelength (black solid curve), but much less so when plotted against the wavenumber (black dashed curve). The spectral dispersion of a grating, on the other hand, is linear in the wavelength domain (red solid curve), but substantially nonlinear in the wavenumber domain (red dashed curve). The nonlinearity parameter NL used to label the grating curves is defined in (2) and (3).

grating dispersion. Other glasses show a similar shape. Since a prism's angular dispersion is nonlinearly related to the glass dispersion, the linearity of $n(\sigma)$ is not by itself enough to provide linear-in-wavenumber spectral dispersion.

In Paper I we presented a design procedure for direct-vision doublet and double-Amici dispersive prisms, and then adapted the procedure to triplet and Janssen prisms in Paper II. There we showed that the additional degrees of freedom available to triplet prisms above those of the better known double-Amici prisms allows a designer to improve on dispersion linearity while maintaining other prism characteristics. The designs presented in Paper II achieved a limited success in modeling prisms with linear dispersion in the wavelength domain. With the switch to the wavenumber domain, achieving linearity is much easier, so that it becomes possible to design prisms with negligible nonlinearity.

The nonlinear equation relating the deviation angle δ to the prism design parameters can be derived by concatenating the refraction equation (using Snell's law) at each interface. For a triplet compound prism, the refraction equations are

$$\left.\begin{aligned}
\theta_1 &= \theta_0 + \beta_1 & \theta_3' &= \arcsin(\tfrac{n_2}{n_3}\sin\theta_3)\\
\theta_1' &= \arcsin(\tfrac{1}{n_1}\sin\theta_1) & \theta_4 &= \theta_3' - \alpha_3\\
\theta_2 &= \theta_1' - \alpha_1 & \theta_4' &= \arcsin(n_3\sin\theta_4)\\
\theta_2' &= \arcsin(\tfrac{n_1}{n_2}\sin\theta_2) & \theta_5 &= \theta_4' + \gamma_3\\
\theta_3 &= \theta_2' - \alpha_2
\end{aligned}\right\}, \quad (1)$$

where $\beta_1 = \alpha_1 + \frac{1}{2}\alpha_2$ and $\gamma_3 = \alpha_3 + \frac{1}{2}\alpha_2$. All of the quantities used here are defined in Fig. 2. The angles θ_i and θ_i' are the angles of incidence and refraction at interface i, and the ray deviation angle δ is defined as $\delta = \theta_0 - \theta_5$. The quantities $n_i(\lambda)$ and α_i are the glass refractive indices and prism apex angles. The deviation angle is thus a nonlinear function of all of these parameters, $\delta(n_1(\lambda), n_2(\lambda), n_3(\lambda), \alpha_1, \alpha_2, \alpha_3, \theta_0)$. For a double-Amici prism, $\alpha_3 = \alpha_1$ and $n_3(\lambda) = n_1(\lambda)$.

Modifying the prism design algorithms from Papers I and II for wavenumber-sampled data is simple: one need only sample the glass refractive indices at uniformly spaced wavenumbers within the same spectral range. Writing the dependence explicitly, the nonlinearity penalty term in the merit function for each setup becomes

$$\mathrm{NL}_\lambda = \int \left|\frac{d^2\delta}{d\lambda^2}\right| \mathrm{d}\lambda, \quad (2)$$

or

$$\mathrm{NL}_\sigma = \int \left|\frac{d^2\delta}{d\sigma^2}\right| \mathrm{d}\sigma, \quad (3)$$

where the merit function is written as

$$M_{\mathrm{nl}} = M_0 + w_{\mathrm{nl}}\mathrm{NL}, \quad (4)$$

with NL_λ or NL_σ in the place of NL depending on whether λ or σ space is uniformly sampled. The "base" merit function M_0 is

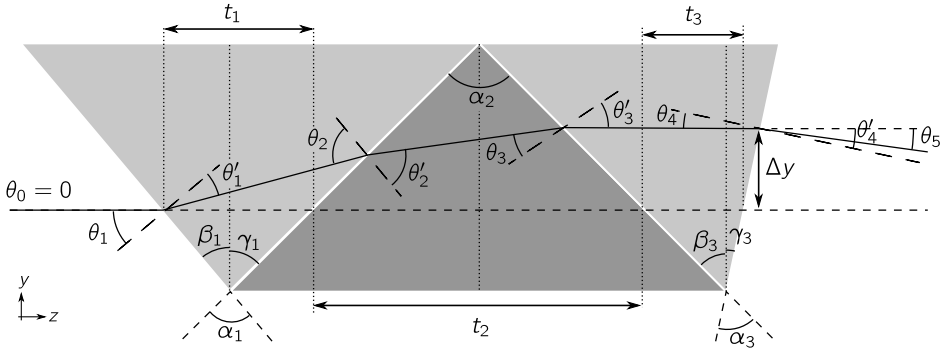

Fig. 2. Example triplet compound prism, where the second element is assumed to be oriented symmetrically with respect to the optical axis normal. The system shown here has prism apex angles $(\alpha_1, \alpha_2, \alpha_3) = (-85°, 90°, -55°)$, beam displacement Δy, and axial thicknesses t_1, t_2, and t_3. For this example, the input ray has an angle $\theta_0 = 0°$, such that $\delta = 15°$.

$$M_0 = (\bar{\delta} - \bar{\delta}^*)^2 + (\Delta - \Delta^*)^2 + \Theta^2. \quad (5)$$

Here $\bar{\delta}$ is the ray deviation angle for the central wavenumber (i.e., $\bar{\delta} \equiv \delta(\bar{\sigma})$ for $\bar{\sigma} = (\sigma_{\min} + \sigma_{\max})/2$), Δ is the spectral dispersion ($\Delta \equiv \delta(\sigma_{\max}) - \delta(\sigma_{\min})$), Θ is a penalty term for large ray incidence angles (see Eq. 12 of Paper I), and w_{nl} is the relative weight applied to the nonlinearity penalty. In order to clearly discriminate between the linear-in-wavelength dispersion discussed in Paper I and the linear-in-wavenumber dispersion discussed here, we define the terms "λ-linearity" quantified by NL_λ, and "σ-linearity" by NL_σ, where the subscript indicates in which space the function is uniformly sampled.

Using the same system parameters as the λ-linearized designs in Tables 1 and 2 of Paper I, Table 1 below shows the results of designing prisms for σ-linearized dispersion. All of the designs in Table 1 have been restricted to ray angles of incidence less than 65° at all prism interfaces. In the doublet prisms of section (a), σ-linearity improvement is achieved by pairing two glasses with nearly identical refractive indices but substantially different dispersions. This setup produces equal and opposite ray deviation at the first and last interfaces of the prism, but dispersion without deviation at the central interface. The double-Amici and triplet designs follow a different principle, pairing a very low dispersion glass with an LAF or LAK material. (Other glass combinations will work, but these produce the best dispersion linearity.) Note that in all of the tabulated data below, we remove the prefixes on the glass names (i.e., N-BK10 is written as BK10) in order to keep the tables compact. In some cases, we have also abbreviated names, such as LITHOSIL-Q/LITHQ, LITHOTEC-CAF2/CAF2, CLEARTRAN/CLEAR, and ZNS_BROAD/ZNSBR.

In addition to the nonlinearity value NL, two convenient measures of a prism design are the spectral sampling ratio (SSR) and the beam compression factor K. SSR is a measure introduced in Paper I (Eq. 1) to describe how much the spectral bands are stretched by nonlinear dispersion, whereas K (introduced in Eq. 2 of Paper II) indicates the change in beam width between the incident and exiting beams. Typically, one wishes to have SSR = 1 and $K \geq 0.9$, as these two values correspond to highly linear spectral dispersion and to a beam experiencing little compression along the spectral spread axis.

While the designs of section (b) in Table 1 show larger nonlinearity values than those of section (a), this is a result of a higher dispersion target. (A double-Amici prism designed to the same target values as a doublet will almost always have better performance. Exceptions occur when a highly asymmetric layout is needed for good performance.) See Fig. 3 for the resulting dispersion curves of these designs. The prisms of section (c) have dispersion values somewhat lower than the target as a result of the competing terms of the merit function. One can achieve a closer match to the target by increasing the weight of the $(\Delta - \Delta^*)^2$ term in M_{nl} relative to w_{nl}, although at some tradeoff in nonlinearity.

Comparing these results with those of the corresponding tables in Papers I and II, we find that NL_σ is much smaller than the NL_λ values obtained with equivalent prisms:

Prism Type	Paper, Table, Design	Δ^*	NL_λ	NL_σ
Doublet	1,1,6a	1°	0.323	-
Doublet	3,1,1a	1°	-	0.069
Double-Amici	1,2,1a	4°	1.770	-
Double-Amici	3,1,1b	4°	-	0.479
Triplet	2,1,1b	4°	1.762	-
Triplet	3,1,1c	4°	-	0.411

Table 1. Linear-in-Wavenumber Dispersive Prisms for Wideband Visible Wavelength Spectral Interferometry: the Best Performing Prisms are Listed in Order of Dispersion Linearity in the Wavenumber Domain and Optimized over the Schott Glass Catalog [a]

	Prism Type	Glass 1	Glass 2	Glass 3	α_1 (deg)	α_2 (deg)	α_3 (deg)	$\bar{\delta}$ (deg)	Δ (deg)	NL_σ	SSR	K
	merit func: M_0, λ range: 400–700 nm, $\Delta^* = 1°$											
1a.	Doublet	LAF34	SSK5		79.79	−101.86		0.000	1.000	0.069	1.47	0.49
2a.	Doublet	LITHQ	CAF2		93.15	−99.57		0.001	0.990	0.071	1.38	0.84
3a.	Doublet	LAK14	BAK4		77.86	−106.75		0.000	1.000	0.071	1.43	0.40
4a.	Doublet	LASF44	BAF10		76.73	−101.28		0.000	1.000	0.072	1.50	0.47
5a.	Doublet	FK5	CAF2		87.23	−100.72		0.000	1.000	0.076	1.41	0.72
	Merit func: M_0, λ range: 400–700 nm, $\Delta^* = 4°$											
1b.	d-Amici	CAF2	LAK33A		95.25	−94.29		0.000	4.000	0.479	1.89	1.00
2b.	d-Amici	CAF2	LAF34		92.27	−90.42		0.000	4.000	0.506	1.97	1.00
3b.	d-Amici	CAF2	LAF35		92.32	−93.30		0.000	4.000	0.513	1.99	1.00
4b.	d-Amici	CAF2	LAK10		93.73	−96.76		0.000	4.000	0.524	1.98	1.00
5b.	d-Amici	CAF2	LAF21		89.69	−87.15		0.000	4.000	0.528	2.02	1.00
	Merit func: $M_{\mathrm{nl}} + (K-1)^2$, λ range: 400–700 nm, $\Delta^* = 4°$											
1c.	Triplet	LASF41	SK11	PSK53A	−59.61	−10.08	81.20	0.016	3.957	0.411	1.79	0.59
2c.	Triplet	CAF2	LAK34	CAF2	95.55	−97.70	97.39	−0.019	3.901	0.452	1.84	0.95
3c.	Triplet	CAF2	LAK33A	CAF2	95.22	−94.28	95.22	0.000	3.997	0.478	1.89	1.00
4c.	Triplet	FK51A	LAK33A	CAF2	93.00	−97.67	94.99	−0.003	3.901	0.487	1.95	0.95
5c.	Triplet	CAF2	LAK33A	PK51	92.90	−101.67	95.91	−0.004	3.906	0.494	1.96	0.95

[a] All of the designs are nondeviating ($\delta^* = 0$), assume axial illumination ($\theta_0 = 0$), and are constrained to angles of interface <65°. The dispersion gradient curves of all 10 prisms are illustrated in Fig. 3 together with the layouts of prisms 1*a* and 1*b*.

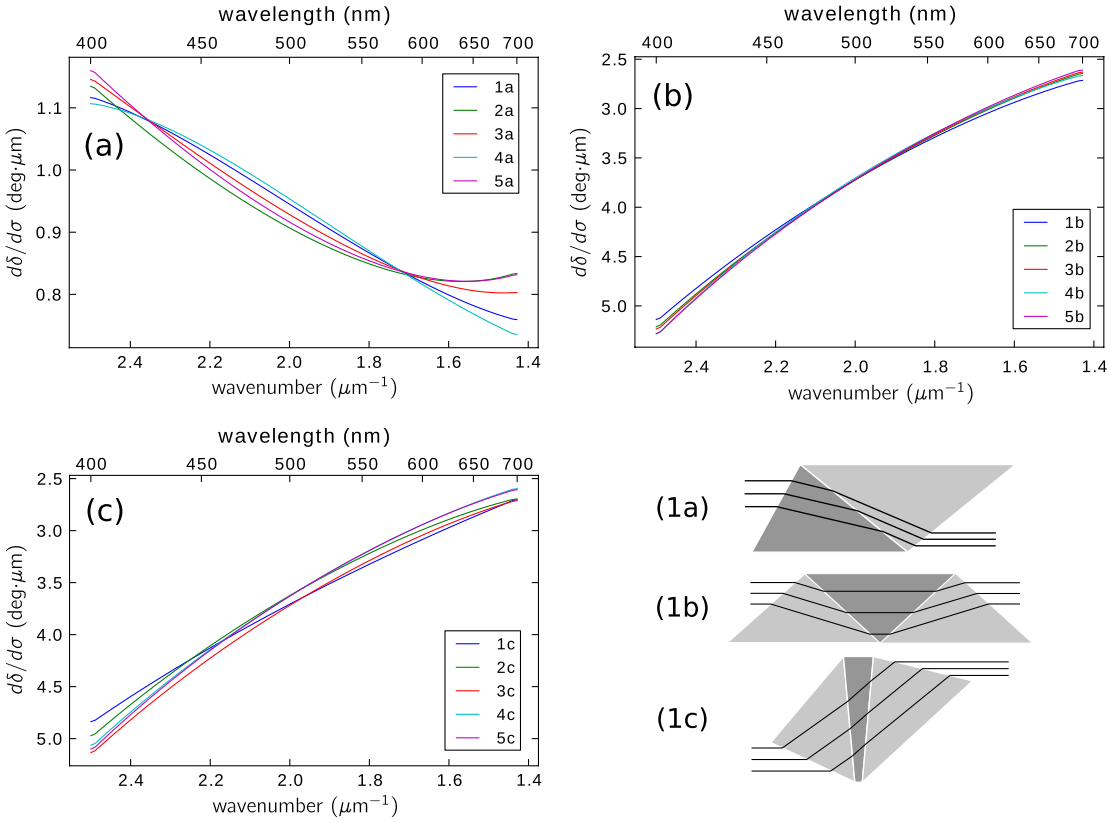

Fig. 3. (Color online) Layouts and dispersion gradient, $d\delta/d\sigma$, of the designs shown in Table 1 (only three representative layouts are shown). (a) $\Delta = 1°$ doublets, (b) $\Delta = 4°$ double-Amici prisms, (c) $\Delta = 4°$ triplets. Ideal linear dispersion produces a horizontal line in these plots, so that any variation from that line represents the nonlinear dispersion. Note that the spectra here are sampled uniformly in wavenumber; the corresponding wavelength labels are given on the upper x axis for reference.

3. Prism Designs for Spectral Domain OCT

One of the most important applications for σ-linear dispersion is spectral domain OCT [5–8], which is typically performed in the near-IR or short-wave IR (850, 1060, and 1300 nm are common choices for the central wavelength), where penetration depth into tissue is substantially greater than in the visible. However, the dispersion of commonly available glasses is generally much smaller, and the spectral ranges used in OCT (typically 20–100 nm FWHM) are also generally narrower than those used for general purpose spectrometry. This combination of narrow spectral range and greatly reduced dispersion makes dispersive prism design a challenge. For example, a typical OCT setup may use a 75–100 mm focal length lens and a 1024-element detector array with 10 μm pixels, so that an angular dispersion of $\Delta = 5.9°$–$7.8°$ is required. With diffraction gratings, this can be achieved with a groove density of 500–3500 lines per mm(see Appendix A), depending on the spectral width (20 or 100 nm FWHM) and focal length used. Prisms generally require a wide spectral range in order to achieve sufficient dispersion, and so we aim for 6°–8° dispersion across spectral ranges of at least 100 nm—a setup which aims for a mean spectral sampling rate of $\Delta\lambda \approx 0.1$ nm, and thus a maximum imaging depth of [9] $z_{\max} = \bar{\lambda}^2/(4n\Delta\lambda) \approx 1.2$ mm in biological tissue ($n \approx 1.45$).

If the 6°–10° dispersion used for the prism design is insufficient for a given OCT instrument, another means of achieving sufficient sampling is to increase the focal length of the spectrometer's reimaging lens. Since most spectral domain OCT systems operate with diffraction-limited imaging, simply increasing the focal length causes a corresponding increase in the size of the focal spot, so that one must also increase the size of the beam by using a larger aperture objective lens (i.e., a lens with a longer focal length but the same NA). The trade-off is that a higher quality objective lens is needed.

Table 2 shows a number of prisms designed for σ-linearized dispersion with parameters appropriate for use in retinal OCT systems, with spectral ranges centered at 850 nm. Designs in sections (a) and (b) of the table are for a 6° and 8° dispersion angle, while the designs in (c) and (d) use wider spectral ranges and are for 10° dispersion. Until now, the algorithm has constrained the ray angles of incidence in the prisms to $\theta \le 65°$. For the double-Amici designs used here, however, the dispersion targets used in Table 2 are no longer obtainable with this constraint when using the ZEMAX Infrared catalog glasses. Thus, the double-Amici designs in Table 2 use $\theta_{\text{lim}} = 70°$ instead in order to allow sufficient dispersion. Although the triplet prisms, on the other hand, have

Table 2. OCT Prism Designs: the Best Performing Three-Element Prisms Listed in Order of Dispersion σ-Linearity, for $\delta^* = 0$ and $\theta_0 = 0$, and optimized (for sections (a)–(c)) over the ZEMAX Infrared Glass Catalog. Section (d) Optimizes over the Combined Schott Catalog and Infrared Catalog [a]

	Prism Type	Glass 1	Glass 2	Glass 3	α_1 (deg)	α_2 (deg)	α_3 (deg)	$\bar{\delta}$ (deg)	Δ (deg)	NL_σ ($\times 10^4$)	SSR	K
				Merit func: $M_{nl} + (K-1)^2$, λ range: 800–900 nm, $\Delta^* = 6°$								
1a.	d-Amici	ZBLA	ZNSE		103.26	−66.40		0.018	5.889	0.031	1.01	1.00
2a.	d-Amici	BAF2	KRS5		100.03	−62.31		0.000	5.999	0.032	1.02	1.00
3a.	d-Amici	KCL	KRS5		101.02	−63.74		0.001	6.000	0.034	1.02	1.00
4a.	d-Amici	F_SILICA	KRS5		100.80	−61.37		0.039	5.789	0.034	1.03	1.00
5a.	d-Amici	ZBLAN	KRS5		100.59	−63.11		0.001	6.000	0.034	1.02	1.00
6a.	Triplet	CAF2	KRS5	IRG9	100.67	−61.35	99.93	−0.003	5.985	0.031	1.02	0.99
7a.	Triplet	CAF2	KRS5	ZBLAN	100.61	−61.22	100.20	−0.004	5.971	0.031	1.01	0.97
8a.	Triplet	IRG9	ZNSE	IRG15	102.58	−65.16	103.23	0.003	5.907	0.031	1.01	0.91
9a.	Triplet	SRF2	KRS5	F_SILICA	100.25	−60.50	100.74	−0.003	5.945	0.032	1.01	0.95
10a.	Triplet	BAF2	KRS5	BAF2	100.03	−62.32	100.03	0.000	6.000	0.032	1.02	1.00
				Merit func: $M_{nl} + (K-1)^2$, λ range: 800–900 nm, $\Delta^* = 8°$								
1b.	d-Amici	IRGN6	KRS5		103.23	−72.34		0.002	8.000	0.068	1.03	1.00
2b.	d-Amici	GEO2	KRS5		103.59	−73.75		−0.002	7.998	0.073	1.03	1.00
3b.	d-Amici	IRG7	KRS5		104.33	−70.86		0.001	8.000	0.083	1.03	1.00
4b.	d-Amici	IRGN6	ZNSE		106.35	−72.36		0.049	7.795	0.107	1.05	1.00
5b.	d-Amici	IRG15	KRS5		104.27	−68.74		−0.000	7.999	0.112	1.06	1.00
6b.	Triplet	BAF2	ZNSE	BEO	106.30	−72.59	103.83	−0.001	7.931	0.068	1.02	0.92
7b.	Triplet	BEO	KRS5	IRG9	100.56	−73.13	104.03	0.000	8.000	0.068	1.02	1.00
8b.	Triplet	IRG9	KRS5	CALCITE	105.00	−71.31	102.37	−0.001	8.001	0.069	1.03	1.00
9b.	Triplet	IRG9	ZNSE	MGO	106.89	−73.78	104.32	0.005	7.929	0.069	1.03	0.92
10b.	Triplet	CALCITE	KRS5	IRG15	102.63	−72.97	104.48	0.000	8.000	0.069	1.03	1.00
				Merit func: $M_{nl} + (K-1)^2$, λ range: 750–1050 nm, $\Delta^* = 10°$								
1c.	d-Amici	CAF2	SRTIO3		102.58	−65.26		0.001	9.999	0.218	1.07	0.97
2c.	d-Amici	CAF2	SRTIO3		102.59	−65.27		0.000	10.001	0.218	1.08	0.97
3c.	d-Amici	SRF2	SRTIO3		102.58	−65.59		−0.002	9.999	0.220	1.08	0.97
4c.	d-Amici	KCL	SRTIO3		103.50	−70.09		0.002	9.999	0.246	1.10	0.97
5c.	d-Amici	BAF2	SRTIO3		101.81	−68.23		−0.001	10.000	0.262	1.08	0.97
6c.	Triplet	CAF2	CLEAR	SRF2	103.86	−67.73	106.39	−0.010	9.909	0.184	1.09	0.84
7c.	Triplet	LIF	SRTIO3	CAF2	101.66	−63.32	102.86	−0.006	9.931	0.200	1.07	0.88
8c.	Triplet	BAF2	ZNSBR	LIF	103.94	−67.89	107.87	−0.008	9.916	0.201	1.10	0.85
9c.	Triplet	CAF2	SRTIO3	LIF	101.79	−63.58	103.71	−0.007	9.960	0.208	1.06	0.94
10c.	Triplet	CAF2	CLEAR	KCL	105.06	−70.13	106.67	−0.008	9.914	0.215	1.10	0.84
				Merit func: $M_{nl} + (K-1)^2$, λ range: 400–1050 nm, $\Delta^* = 10°$								
1d.	d-Amici	MGF2	LAK33A		109.63	−94.86		0.000	9.998	1.682	2.16	1.00
2d.	d-Amici	MGF2	LAF34		107.90	−92.32		0.002	10.000	1.770	2.33	1.00
3d.	d-Amici	MGF2	LAF21		106.30	−90.13		−0.001	10.001	1.825	2.38	1.00
4d.	d-Amici	MGF2	LAF35		108.26	−95.03		−0.003	10.000	1.844	2.40	1.00
5d.	d-Amici	MGF2	LAK10		108.92	−97.53		−0.001	9.872	1.850	2.29	1.00
6d.	triplet	GEO2	SAPPHIRE	MGF2	79.45	−18.89	−71.98	0.014	9.868	0.726	1.43	0.53
7d.	Triplet	F5	LAK9	MGF2	83.83	−27.67	−66.93	0.019	9.857	0.853	1.55	0.57
8d.	Triplet	F5	ALON	IRG9	67.62	4.75	−82.34	0.031	9.845	0.869	1.39	0.52
9d.	Triplet	F5	LAK14	MGF2	83.45	−26.90	−67.30	0.022	9.854	0.874	1.58	0.57
10d.	Triplet	LASF44	BAF2	SAPPHIRE	76.56	−13.12	−71.23	−0.073	9.840	0.878	1.60	0.52

[a]All designs have been constrained to angles of incidence $<70°$.

no difficulty achieving the design targets under a 65° constraint, the triplets in Table 2 use $\theta_{lim} = 70°$ for easy comparison with the double-Amici designs.

The results of Table 2 show that the prisms in the 800–900 nm spectral range can achieve a spectral sampling rate $d\delta/d\sigma$ which varies by no more than 2% across the entire spectral range. The prisms in sections (c) and (d), however, have a more restrictive design space and thus have much higher dispersion nonlinearity.

In the 800–900 nm spectral range, all of the designs of Table 2 use either KRS5 (thallium bromo-iodide) or ZNSE (zinc-selenide) glass, the two most dispersive amorphous materials of the Infrared catalog in this spectral range. The design targets for the 750–1050 nm spectral range, despite having a higher dispersion angle, are easier for prisms to achieve and so we see that SRTIO3 and CLEARTRAN become the preferred materials in section (c) due to their lower dispersion nonlinearity than KRS5 and ZNSE. In general, we can also see that due to the restriction on beam compression, triplet prisms provide only a marginal improvement over double-Amici designs for the requirements used here.

In the widest spectral range (400–1050 nm), the triplet designs provide a large improvement in nonlinearity over the double-Amici designs, though at the cost of compressing the beam in the dispersion

axis by 50%. As one increases the weight of the beam compression penalty relative to the other terms of the merit function, the resulting K value of the best designs comes closer to 1, but the NL and SSR values also come closer to the values of the double-Amici designs.

There exist some extraordinarily dispersive materials in the 800–900 nm spectral range: the chalcogenides proustite (silver sulfarsenide, $AgAsS_3$) and silver gallium selenide ($AgGaSe_2$) have about twice the dispersion of KRS5. Both of these crystals have an absorption band in the red end of the visible spectrum, and thus appear a deep red color to the eye. Unfortunately, these crystals are strongly birefringent, making their implementation in spectrometers problematic. There are amorphous materials of similar composition [10], but these are not widely available.

The types of light sources, which can be used for these spectral ranges for OCT, would include superluminescent diodes (e.g., Superlum T870-HP), thermal sources [11–13] (e.g., a Tungsten-Halogen bulb, or Xenon lamp), or tunable Ti:sapphire lasers. In the 800–900 nm spectral ranges, near-IR optimized silicon detector arrays are ideal, whereas for the 400–1050 nm spectral range a deep-depletion silicon CCD [14] is an ideal detector. For the 750–1050 nm range, either a deep-depletion Si CCD, or a Ge, InSb, or HgCdTe detector array is needed.

4. OCT Prisms for Longer Wavelengths

To show that prisms can be used for the longer wavelength spectral ranges analyzed by spectral domain OCT, Table 3 presents a number of prism designs tailored to the spectral ranges of three commercially available wideband superluminescent diodes. Achieving 6° of angular dispersion for wavelengths beyond 1 μm generally requires a spectral band which is at least 150 nm wide, and this has defined the commercial sources we show here for our example designs. Thus, for example, the spectral band of section (a), 1.175–1.425 μm, can be used with the Thorlabs LS2000B superluminescent diode, the 1.21–1.41 μm band of section (b) with InPhenix's IPSDD1308, and the 1.25–1.50 μm range of section (c) with Superlum's Q1350-HP.

The results of using the double-Amici and triplet prism design algorithms for these spectral ranges

Table 3. OCT Prism Designs: the Best Performing Double-Amici Prisms Listed in Order of Dispersion σ-Linearity, for $\delta^* = 0$ and $\theta_0 = 0$ Optimized over the ZEMAX Infrared Glass Catalog [a]

	Prism Type	Glass 1	Glass 2	Glass 3	α_1 (deg)	α_2 (deg)	α_3 (deg)	$\bar{\delta}$ (deg)	Δ (deg)	NL_σ ($\times 10^4$)	SSR	K
					Merit func: $M_{nl} + (K-1)^2$, λ range: 1.175–1.425 μm, $\Delta^* = 6°$							
1a.	d-Amici	KCL	CDSE		100.72	−62.36		−0.001	0.139	0.570	1.14	1.00
2a.	d-Amici	BAF2	CDSE		100.51	−61.47		0.001	0.157	0.587	1.16	1.00
3a.	d-Amici	KBR	AMTIR1		101.94	−65.81		0.000	0.170	0.601	1.17	1.00
4a.	d-Amici	NACL	AMTIR1		101.69	−64.88		0.000	0.172	0.604	1.17	1.00
5a.	d-Amici	KBR	CDSE		100.10	−66.81		0.000	0.190	0.624	1.19	1.00
6a.	Triplet	IRG9	KRS5	KCL	103.98	−67.96	108.82	−0.066	6.029	0.034	1.03	0.69
7a.	Triplet	IRG9	KRS5	BAF2	103.71	−67.41	108.51	−0.001	5.928	0.052	1.05	0.70
8a.	Triplet	F_SILICA	SRTIO3	IRG11	110.54	−81.09	111.38	−0.005	5.946	0.055	1.03	0.68
9a.	triplet	NACL	AMTIR1	MGF2	99.61	−59.23	104.38	0.096	5.915	0.098	1.10	0.87
10a.	triplet	KBR	KRS5	CSBR	107.02	−78.11	105.89	0.006	5.908	0.126	1.13	0.94
					Merit func: $M_{nl} + (K-1)^2$, λ range: 1.21–1.41 μm, $\Delta^* = 6°$							
1b.	d-Amici	NACL	CDSE		103.83	−67.82		0.001	6.001	0.074	1.06	1.00
2b.	d-Amici	KBR	CDSE		104.00	−68.73		0.000	6.001	0.076	1.07	1.00
3b.	d-Amici	CSBR	AMTIR1		102.80	−75.81		0.015	5.871	0.160	1.16	1.00
4b.	d-Amici	CSBR	CDSE		101.22	−77.40		0.002	6.000	0.175	1.18	1.00
5b.	d-Amici	GEO2	AMTIR1		105.61	−71.01		0.033	5.824	0.198	1.21	1.00
6b.	Triplet	KBR	CDSE	CAF2	102.21	−64.42	105.49	−0.006	5.904	0.040	1.02	0.91
7b.	Triplet	KBR	CDSE	SRF2	102.29	−64.58	105.45	−0.007	5.908	0.040	1.03	0.91
8b.	Triplet	KCL	CDSE	IRG9	101.87	−63.74	104.97	0.050	6.081	0.044	1.03	0.80
9b.	Triplet	CSBR	CDSE	MGF2	102.02	−67.61	107.09	−0.000	6.000	0.045	1.03	1.00
10b.	triplet	CSBR	AMTIR1	SRF2	103.29	−68.18	107.14	0.001	6.001	0.048	1.03	1.00
					Merit func: $M_{nl} + (K-1)^2$, λ range: 1.25–1.50 μm, $\Delta^* = 6°$							
1c.	d-Amici	KBR	CDSE		103.26	−68.54		0.000	6.001	0.124	1.12	1.00
2c.	d-Amici	NACL	CDSE		103.12	−67.65		0.001	6.000	0.129	1.13	1.00
3c.	d-Amici	CSBR	AMTIR1		102.39	−75.79		0.000	6.001	0.210	1.22	1.00
4c.	d-Amici	CSBR	CDSE		100.35	−77.19		0.002	6.000	0.221	1.23	1.00
5c.	d-Amici	GEO2	AMTIR1		105.64	−71.15		0.016	5.886	0.304	1.33	1.00
6b.	Triplet	SRF2	KRS5	ZBLA	104.03	−68.07	110.40	0.061	5.976	0.024	1.02	0.53
7b.	Triplet	KBR	CDSE	MGF2	101.21	−62.42	106.41	−0.078	5.987	0.049	1.04	0.85
8b.	Triplet	IRG9	SRTIO3	BEO	108.40	−83.94	111.38	−0.019	6.061	0.050	1.02	0.58
9b.	Triplet	KCL	CDSE	KCL	101.80	−63.60	103.79	−0.014	6.011	0.067	1.05	0.87
10b.	Triplet	CSBR	AMTIR1	MGF2	103.07	−66.29	108.01	0.000	6.000	0.072	1.07	1.00

[a] All designs have been constrained to angles of incidence $< 70°$.

are shown in Table 3. We can see that the dispersion nonlinearity for the double-Amici prisms is substantially higher than it was for the 800–900 nm spectral range used for the retinal OCT prisms. If, however, we compare the triplet designs here with those of Table 2, we find only slight differences—at these longer wavelengths the triplets can provide a substantial improvement in dispersion σ-linearity over their double-Amici counterparts. If one wishes to use these prisms to eliminate the interpolation step typically used in OCT reconstruction algorithms, then the latter can provide data with minimal artifacts.

A remarkable feature of the designs in Table 3 is that all of them share an almost identical layout, regardless of the spectral ranges used. In each of the three example spectral ranges, one can find designs in which the spectral sampling rate varies by no more than 3% across the full spectral range, albeit with some trade-off in beam compression.

CDSE and AMTIR1 are used for the central element of most of the designs in Table 3, whereas there is considerable variety in the materials used for the outer elements. For the three spectral ranges used here, CDSE and AMTIR1 are the most dispersive materials in the Schott and Infrared catalogs used.

5. Engineering Issues for Prism Selection

In addition to factors such as dispersion nonlinearity and prism thickness, there are important engineering issues which may decide whether a given prism design is optimal for a system. These can include the price of obtaining optical quality material (ZnSe, for example, is typically more than 10 times the price of common borosilicate glasses), and properties such as hygroscopy, water solubility, birefringence, thermal stability, toxicity, and corrosiveness.

Hygroscopy describes a material's tendency to take up water from its environment, causing a change in the material optical properties. This can occur either through direct contact with water (as is common in biological imaging) or through exposure to humid air, protection against which requires a sealed environment. Since dispersive prisms are rarely used in water contact, water solubility is less important than hygroscopy *per se*, though the two properties are closely linked. The materials used in the prism designs of Tables 2 and 3, which have significant hygroscopy, are BAF2, CSBR, KBR, KCL, LIF, MGO, and NACL.

Prism birefringence is another property which can cause difficulty to a spectrometer, due to the difference in dispersion values between the ordinary and extraordinary beams transmitted by the material. While one can compensate for this to some extent by cutting each single prism element as two symmetric pieces from orthogonal crystal orientations, an easier solution is of course to avoid birefringent materials in the design. Birefringent materials used in the prism designs of Tables 2 and 3 include BEO (0.0156), CALCITE (–0.172), CDSE (0.02), and MGF2 (0.0118), where the parenthetical values give the amount of birefringence Δn at $\lambda = 1\,\mu$m.

Among IR-transmitting glasses, toxicity is another important material characteristic, and is a property that can also influence cost and material availability. Toxic materials used in the prism designs of Tables 2 and 3 include CDSE, CSBR, KBR, KCL, and KRS5. In general, robust coatings of such materials can make them safe for general laboratory use, but their toxicity prior to coating restricts the manufacture of prisms made from them to specialized optics companies.

6. Conclusion

The OCT prism designs provided in Tables 2 and 3 show that it is possible to provide practical direct-vision OCT prisms in which the angular dispersion is sufficiently linear-in-wavenumber to minimize or eliminate the commonly used interpolation step (from wavelength to wavenumber sampling) prior to fast Fourier transform computation [4,5]. Moreover, the use of prism dispersers in place of gratings allow system designers to reduce stray light, to improve optical throughput, and to use the convenient direct-view geometry. Despite these advantages, some difficulties remain for using compound prisms in OCT. Although one can achieve substantial dispersion with these elements, their dispersive power remains weaker than their grating counterparts, so that a relatively wide spectral range is needed in order to achieve sufficient sampling of the spectrum. One can, in general, compensate for this by using longer focal lengths for both the objective lens and for the spectrometer's reimaging lens while maintaining the objective lens' NA. The main trade-off in this approach is a reduction in the depth of focus, which causes signal loss for measuring reflections from surfaces deep within the sample.

The algorithms used for designing the OCT prisms use the techniques discussed extensively in Paper I and II, in which a nonlinear optimization routine is used directly on the prism refraction Eq. (1) to iteratively locate a solution. In order to restrict the algorithm to practical prism designs, several modifiers are added to the optimizer merit function such as a penalty on beam compression and a penalty on dispersion nonlinearity, in addition to the standard merit function terms (5). While all of the achievements of the customized design algorithms we use here are possible using standard optical design software, our algorithms provide an easier interface for manipulating the low-level features of the software, such as the optimization algorithm, the various features of the merit function, such as the penalty terms, and also allow use of a wide suite of numerical- and text-manipulation functions available in a high-level and powerful language. We encourage interested readers to download and modify the design code we have written for this work, available at the authors' website [15]. The entire suite of functions is written in Python using standard modules.

Appendix A: Deriving the Grating Groove Density from Angular Dispersion

The basic diffraction grating equation in air is $G \sin \delta = m\lambda$, where G is the spacing between grooves, δ is the ray deviation angle, m is the diffraction order, and λ is the wavelength. Taking the derivative of this equation and assuming small angles gives the dispersion equation $\Lambda \approx m d\delta/d\lambda$, where $\Lambda = 1/G$ is the grating groove density (typically expressed in lines per millimeter). Using the nomenclature of Section 2, and assuming the first diffraction order, we can write this as $\Lambda \approx \Delta/\lambda_{\text{range}}$, where $\lambda_{\text{range}} = \lambda_{\max} - \lambda_{\min}$. In a spectrometer, the linear diffraction length at the detector is given as $\tan(\Delta/2) = Nx/(2f)$, where N is the number of detector pixels, x is the pixel pitch, and f is the spectrometer's reimaging lens focal length. Again, assuming small angles, we can combine the two equations to obtain

$$\Lambda \approx \frac{Nx}{f\lambda_{\text{range}}}.$$

This is the equation used to obtain the diffraction grating examples of Section 3, where we assumed that the detector would see a full spectral range of twice the FWHM of the source spectral width (i.e., $\lambda_{\text{range}} = 2\,\text{FWHM}$).

This work was partially supported by the National Institutes of Health (NIH) grants RO1-CA124319 and R21-EB009186.

References

1. N. Hagen and T. S. Tkaczyk, "Compound prism design principles, I," Appl. Opt. **50**, 4998–5011 (2011).
2. N. Hagen and T. S. Tkaczyk, "Compound prism design principles, II: triplet and Janssen prisms," Appl. Opt. **50**, 5012–5022 (2011).
3. K. Oka and T. Kato, "Spectroscopic polarimetry with a channeled spectrum," Opt. Lett. **24**, 1475–1477 (1999).
4. C. Dorrer, N. Belabas, J.-P. Likforman, and M. Joffre, "Spectral resolution and sampling issues in Fourier-transform spectral interferometry," J. Opt. Soc. Am. B **17**, 1795–1802 (2000).
5. Z. Hu and A. M. Rollins, "Fourier domain optical coherence tomography with a linear-in-wavenumber spectrometer," Opt. Lett. **32**, 3525–3527 (2007).
6. C. M. Eigenwillig, B. R. Biedermann, G. Palte, and R. Huber, "K-space linear Fourier domain mode locked laser and applications for optical coherence tomography," Opt. Express **16**, 8916–8937 (2008).
7. V. M. Gelikonov, G. V. Gelikonov, and P. A. Shilyagin, "Linear-wavenumber spectrometer for high-speed spectral-domain optical coherence tomography," Opt. Spectrosc. **106**, 459–465 (2009).
8. M. Jeon, J. Kim, U. Jung, C. Lee, W. Jung, and S. A. Boppart, "Full-range *k*-domain linearization in spectral-domain optical coherence tomography," Appl. Opt. **50**, 1158–1163 (2011).
9. A. F. Fercher, W. Drexler, C. K. Hitzenberger, and T. Lasser, "Optical coherence tomography—principles and applications," Rep. Prog. Phys. **66**, 239–303 (2003).
10. M. A. Popescu, *Non-Crystalline Chalcogenides* (Springer, 2002).
11. A. F. Fercher, C. K. Hitzenberger, M. Sticker, E. Moreno-Barriuso, R. Leitgeb, W. Drexler, and H. Sattmann, "A thermal light source technique for optical coherence tomography," Opt. Commun. **185**, 57–64 (2000).
12. L. Vabre, A. Dubois, and A. C. Boccara, "Thermal-light full-field optical coherence tomography," Opt. Lett. **27**, 530–532 (2002).
13. B. Laude, A. D. Martino, B. Drévillon, L. Benattar, and L. Schwartz, "Full-field optical coherence tomography with thermal light," Appl. Opt. **41**, 6637–6645 (2002).
14. S. E. Holland, D. E. Groom, N. P. Palaio, R. J. Stover, and M. Wei, "Fully depleted, back-illuminated charge-coupled devices fabricated on high-resistivity silicon," IEEE Trans. Electron Devices **50**, 225–238 (2003).
15. URL: http://www.owlnet.rice.edu/~tt3/.